ACS OMEGA

Open Access

http://pubs.acs.org/journal/acsodf

Article

Antimicrobial Peptide Fusion and Alginate Encapsulation Broaden the Antibacterial Spectrum and Preserve Storage Stability of the Endolysin *Ab*Lys1 from *Acinetobacter baumannii* Phage *Ab*TZA1

Georgios E. Premetis, Panagiota Pantiora, Nirmal Poudel, Nikolaos Georgakis, Eleni Aikaterini Tzanetopoulou, Anastassios C. Papageorgiou, and Nikolaos E. Labrou*

Cite This: *ACS Omega* 2026, 11, 35326−35336

Read Online

ACCESS | Metrics & More | Article Recommendations | Supporting Information

ABSTRACT: The emergence of multidrug-resistant (MDR) bacterial pathogens, particularly *Acinetobacter baumannii*, has necessitated the development of novel antimicrobial strategies. Endolysins, which are bacteriophage-derived peptidoglycan hydrolases, have shown promise as alternative therapeutics against antibiotic-resistant bacteria. The endolysin *Ab*Lys1 from *A. baumannii* phage TZA1 belongs to the glycoside hydrolase family 24 (GH24) and displays high selectivity and bacteriolytic activity against the Gram-negative *A. baumannii*. In this study, an engineered form of *Ab*Lys1 was obtained by fusion with an antimicrobial α-helical decapeptide. Compared to the wild-type enzyme, the engineered enzyme exhibited enhanced lytic activity against *A. baumannii* and showed lytic activity against a broader panel of bacterial species, including *Enterococcus* and *Staphylococcus*, as well as *Salmonella* sp., *Klebsiella oxytoca* and *Escherichia coli*, with activity levels varying among strains. In addition, the enzyme exhibited activity against plant pathogens, such as *Pseudomonas syringae* and several *Xanthomonas* strains. The enzyme was encapsulated in an alginate gel matrix (art-*Ab*Lys1-Alg), and its storage stability, bacteriolytic, and antibiofilm activities were investigated. Thermostability analysis revealed that the encapsulated enzyme exhibited a dramatic increase in stability, retaining >75% of its activity after 120 days at 4 °C. In addition, art-*Ab*Lys1-Alg showed an increased biofilm reduction ability for *A. baumannii* biofilm compared to the free enzymes. The findings of this study demonstrate that the combined strategy of antimicrobial peptide (AMP) fusion and alginate encapsulation significantly enhances the functionality and practical applicability of *Ab*Lys1 in diverse biomedical and environmental contexts.

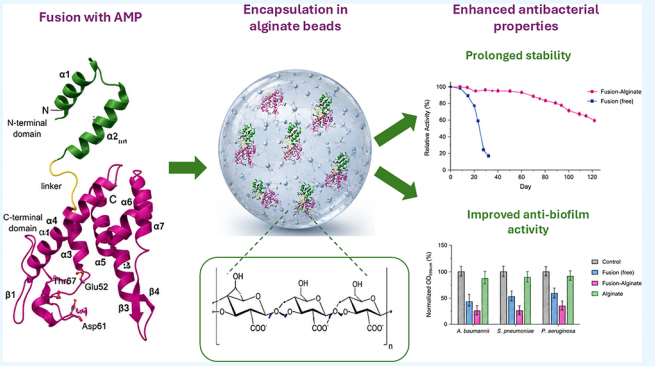

INTRODUCTION

Acinetobacter baumannii is a Gram-negative bacterium, that causes a wide range of severe nosocomial infections, including pneumonia, bacteraemia, urinary tract infections, and other infections through wounds, in immunocompromised patients. The frequency of infections and mortality is higher in intensive care units.[1,2] This pathogen exhibits an impressive ability to develop resistance to almost all commercially available antibiotics, thereby posing a global threat. The excessive clinical use of carbapenems, the most common and effective antibiotics against the pathogen, has led to the development of resistance.[3] To date, therapeutic options for this resistant pathogen remain limited.

Endolysins are phage-derived peptidoglycan-degrading enzymes that have emerged as promising antimicrobial agents.[4,5] Unlike traditional antibiotics, endolysins exhibit rapid bactericidal activity, high specificity, and a low propensity for resistance development, making them valuable tools for combating multidrug-resistant pathogens.[6−9] A notable advancement in endolysin engineering is artilysinization, that is, the fusion of endolysins with peptides or domains, which enables them to breach the outer membrane of Gram-negative bacteria, thereby extending the endolysin spectrum of activity.[4,5,10] Artilysins thus represent a novel class of engineered antimicrobials capable of tackling a broader range of bacterial infections with precision and efficacy than their parent enzymes. Antimicrobial peptides (AMPs) are highly effective tools for the artilysinization of endolysins because their ability to disrupt bacterial membranes facilitates the translocation of endolysins across the outer membrane barrier of Gram-negative bacteria.[11] Recent studies at both therapeutic and molecular levels have demonstrated that AMPs exhibit

Received: January 9, 2026
Revised: May 10, 2026
Accepted: May 19, 2026
Published: June 8, 2026

https://doi.org/10.1021/acsomega.6c00294
ACS Omega 2026, 11, 35326−35336

significant antibacterial activity and serve as alternatives to common antibiotics for multidrug-resistant infections.[12−15] By fusing AMPs with endolysins, engineered artilysins can overcome the intrinsic defense mechanisms of Gram-negative pathogens, significantly broadening the antibacterial spectrum and enhancing the therapeutic potential of endolysin-based antimicrobials.[16,17]

Many natural and synthetic AMPs are highly active against both Gram-positive and Gram-negative bacteria.[13−15,18,19] Antimicrobial peptides with an α-helix motif and amino acid sequence $(XXYY)_n$, where X and Y represent hydrophobic and positively charged amino acids, respectively, have shown significant activity against Gram-positive bacteria, with peptide $(LLKK)_3$ being the most representative example.[20,21]

Alginate, a natural polysaccharide, forms biocompatible and biodegradable hydrogels that can effectively entrap enzymes while maintaining their catalytic activity. Encapsulation serves to enhance enzyme stability, protect against denaturation, and enable controlled and sustained release, thereby improving bioavailability and therapeutic efficacy.[22−27] Alginate is believed to form a protective hydrogel matrix around enzymes, providing hydration and maintaining optimal conditions for enzymatic function, thereby reducing activity loss over time. Moreover, beads and nanoparticles derived from sodium alginate can be formed using simple methods under mild conditions without the need for corrosive chemicals, which could compromise the stability and activity of the enzymes.[26,27]

Recent studies have highlighted the potential of alginate-based formulations to enhance the stability and efficacy of bacteriophage endolysins for biofilm treatment. Ghate et al. (2024) demonstrated that alginate binding improves endolysin stability and potentiates its lytic activity by maintaining a partially folded conformation.[28] Vasina et al. (2024) showed that an alginate gel encapsulated with enzybiotics effectively eradicates multispecies biofilms, offering a promising strategy for combating resistant bacterial communities.[29] Kaur et al. (2020) explored endolysin-loaded alginate−chitosan nanoparticles as potential remedies for *Staphylococcus aureus* infections, highlighting their ability to enhance therapeutic delivery.[22] Collectively, these findings support the role of alginate-based systems in improving endolysin-based antimicrobial therapies for biofilm-associated infections.

Biofilms are highly resistant microbial communities that pose significant challenges in medical, industrial, and environmental settings.[30,31] Their protective matrix shields bacteria from antibiotics, disinfectants, and the immune system, making it difficult to eradicate infections. Effective biofilm treatment requires strategies that can penetrate this matrix and disrupt bacterial cells. Enzymatic approaches using endolysins and other biofilm-degrading enzymes have emerged as promising alternatives to conventional antibiotics.[32−34] These enzymes break down biofilm components, exposing bacteria to antimicrobial agents and enhancing their elimination. Combining enzymatic treatments with physical or chemical methods such as ultrasound or nanoparticles can further improve biofilm disruption.[15,18,29,33,34]

In this study, an engineered form of *Ab*Lys1[35] was created by fusion with an α-helical decapeptide. The engineered enzyme (art-*Ab*Lys1) was stabilized by encapsulation in calcium alginate beads and the antibiofilm potential of the encapsulated enzyme was evaluated. The results suggest that alginate-based encapsulation systems can effectively enhance the stability and efficacy of endolysins, making them promising candidates for developing novel antibacterial strategies.

MATERIALS AND METHODS

Materials

The bacterial strains used have been previously described.[35] Additional strains used included clinically isolated *Enterococcus faecium*, *Salmonella* sp., *Klebsiella oxytoca*, and *Staphylococcus epidermidis* (MRSE, resistant to methicillin, ciprofloxacin, and erythromycin), as well as commercially available *Pseudomonas aeruginosa* ATCC 27853 and *Escherichia coli* DH5α. The following plant pathogens were used: *Clavibacter michiganensis* HMV 4521, *C. michiganensis* HMV 4783, *Pseudomonas syringae*, *Xanthomonas campestris* campestris HMV 84000, *Xanthomonas euvesicatoria* 5075, *X. euvesicatoria* 5071, *Acidovorax citrulli* 55660, and *Xanthomonas citri*.

The Encapsulator B390 (Buchi Corporation, USA) was used for alginate encapsulation experiments. All chemicals used were of analytical grade and obtained from Sigma-Aldrich (USA).

Methods

Fusion of the AMP to the N-Terminus of *Ab*Lys1. Fusion of AMP to the N-terminus of *Ab*Lys1 was performed using PCR. The initial step involved designing primers for the amplification of the pETite-*Ab*Lys1-6×His construct, as previously described.[35] The forward primer contained the nucleotide sequence 5′-TGCCTGCTGAAGAAGCTGCTGAAGAAGTGC-3′ (corresponding to MCLLKKLLKKC) and the first 15 nucleotides of the gene of interest (aa sequence DVKPF) lacking the start codon (ATG). The primer sequences were as follows: 5′-ATGTGCCTGCTGAAGAAGCTGCTGAAGAAGTGCGACGTCAAACCGTTC-3′ and 5′-GAAGGAGATATACATATGTGCCTGCTGAAGAAGCTG-3′. The primers were phosphorylated and the final PCR product was a linear plasmid vector containing the CLLKKLLKKC-flagged gene. PCR was performed in a total volume of 25 μL. PCR contained 10 μM of each primer, 20 ng template DNA, 0.25 mM of each dNTP, 5 μL of 5× KAPA HiFi Fidelity buffer and 0.5 units (U) of KAPA HiFi DNA polymerase (KAPA Biosystems, Wilmington, Delaware, USA). The PCR protocol consisted of 30 cycles of amplification. The initial template denaturation was performed for 3 min at 95 °C, followed by 30 cycles of 20 s at 98 °C, 15 s at 57 °C, and 15 s at 72 °C. A final extension step at 72 °C for 10 min was performed after the 30th cycle. The resulting PCR amplicon was ligated using T4 ligase (TAKARA BIO Inc.). The reaction mix contained 2 μL of the PCR product, 1 μL of 10 ligase reaction solution, 6 μL of sterile ddH_2O, and 1 μL of T4 DNA ligase (350 U/μL) and was incubated at 16 °C for 16 h, followed by enzyme inactivation at 65 °C for 15 min. Finally, 1.5 μL of 10× DNP1 reaction buffer and 0.5 μL of DNP1 (10 U/μL) were added to the ligation mixture to a final volume of 15 μL. The reaction was incubated at 37 °C for 3.5 h and then heated at 80 °C for 20 min to inactivate DNP1. The final reaction product was used to transform *E. coli* cells.

Heterologous Expression in *E. coli* BL21 (DE3) and Purification of art-*Ab*Lys1. Heterologous expression of art-*Ab*Lys1 was carried out in *E. coli* BL21 (DE3), as described for the wild-type enzyme *Ab*Lys1.[35] Purification of art-*Ab*Lys1 was achieved using affinity chromatography on Ni^{2+}-IDA-Sepharose as described previously.[35] The fractions with the highest purity (eluted with 0.15−0.35 M imidazole) were mixed and stored at 4 °C for further studies.

Differential Scanning Fluorimetry (DSF). DSF was used to monitor the thermal denaturation of art-*Ab*Lys1 using SYPRO Orange dye as described previously.[35] The samples were heated from 25 to 95 °C at a constant rate of 1 °C/min. Melting temperatures (T_m) were calculated as an inflection point of the melting curve, assuming a two-state unfolding model, using the Protein Thermal Shift software (Thermo Fisher Scientific). Assays were performed in triplicate.

Enzyme Assays. The Remazol Brilliant Blue-R-labeled peptidoglycan (RBBR-PNG) degradation assay was conducted as previously described.[35] The bacterial lytic activity of art-*Ab*Lys1 was evaluated using turbidity assays as described previously.[35] Suspensions of each

https://doi.org/10.1021/acsomega.6c00294
ACS Omega 2026, 11, 35326−35336

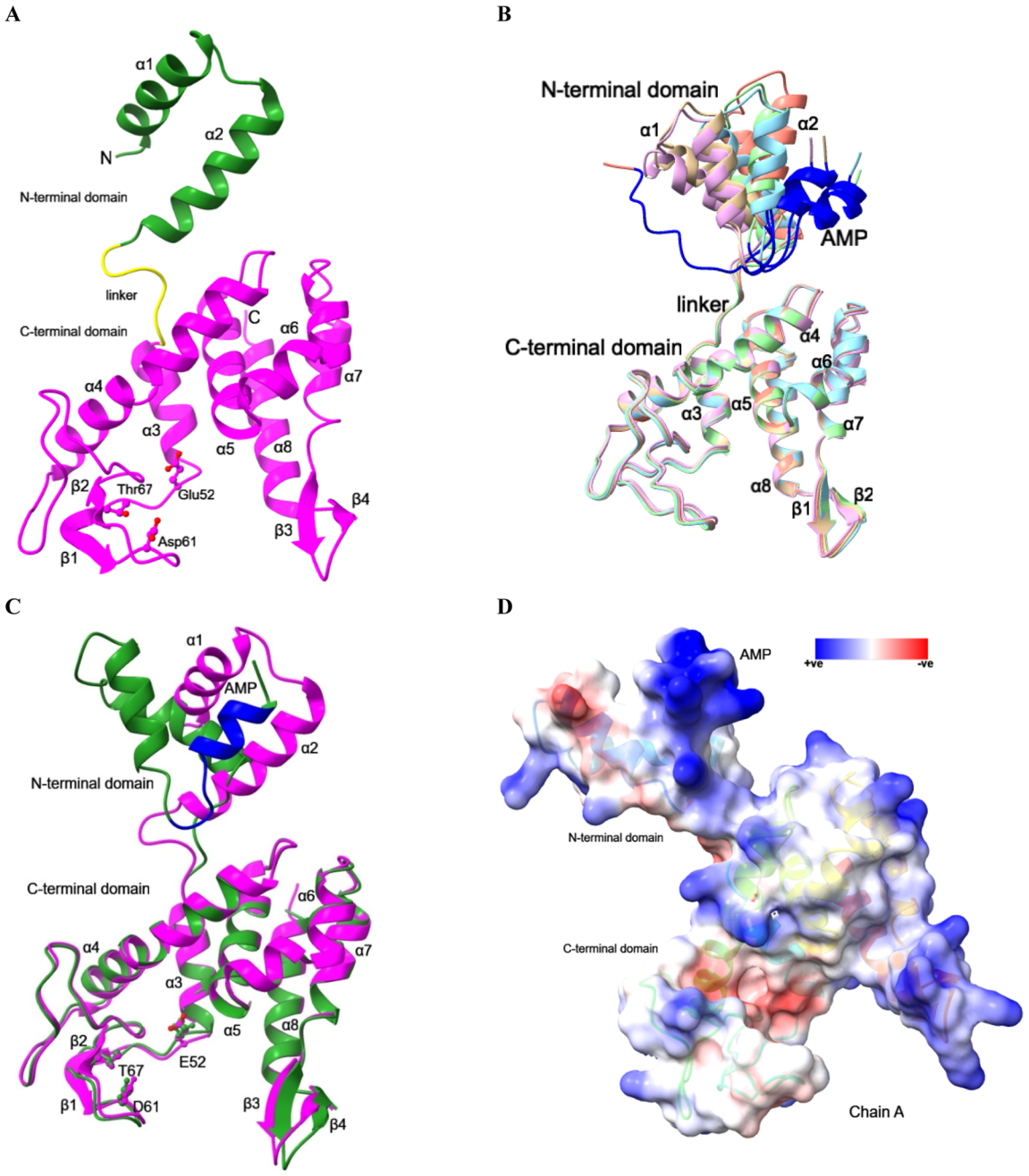

Figure 1. (A) Ribbon diagram of the wild-type *Ab*Lys1 (PDB id: 8APP).[35] Secondary structure elements (SSEs) are labeled. The side chains of active site residues (D61, T67 and E52) are shown in stick representation and labeled. *Ab*Lys1 consists of two distinct domains: an N-terminal peptidoglycan-destabilizing domain and a C-terminal catalytic domain responsible for peptidoglycan hydrolysis. The two domains are linked by a flexible loop that facilitates functional adaptability. (B) Superimposition of the five AF2-generated models of art-*Ab*Lys1. $C(LLKK)_2C$ AMP fused to the N-terminal of *Ab*Lys1 is highlighted in blue. SSEs are labeled for reference. (C) The best predicted AF2 model of art-*Ab*Lys1 (forest green) superimposed onto chain A of the crystal structure of *Ab*Lys1 (magenta; PDB id 8APP). AMP is colored in blue in the art-*Ab*Lys1 model. (D) Electrostatic surface representation of the best predicted art-*Ab*Lys1 AF2 model. The Coulombic surface coloring shows the surface electrostatic potential, blue representing the positive charge, red indicating the negative charge. The molecular visualization software Chimera[43] was used for structure visualization and creation of figures.

strain containing 150 μg of art-*Ab*Lys1 in HEPES buffer (pH 7.5, 50 mM) were prepared in order to achieve a turbidity equivalent of 0.5–0.6 (A_{600nm}). Reactions were incubated at room temperature for 2 h and the reduction in OD_{600nm} was recorded every 10 min.

Antimicrobial Activity Assays Using Disc Diffusion Method. The antimicrobial activity of art-*Ab*Lys1 was measured using the Kirby–Bauer disc diffusion method in agar,[36] as described previously.[35] For all substrates, bacterial cultures were grown in Mueller–Hinton nutrient medium and disks with a diameter of 6 mm were impregnated with different concentrations of art-*Ab*Lys1 (10, 15, 20, 40, and 60 μg). A disk impregnated with elution buffer containing 150 mM imidazole was used as the control. Immediately after plating the Mueller–Hinton medium in Petri dishes, the disks were placed on the surface of the medium, and the plates were incubated for 16 h at 37 °C to allow bacterial growth.

Minimum inhibitory concentration (MIC) was estimated from disk diffusion assays using a diffusion-based model derived from Fick's second law, as described previously.[37−40] Disks containing increasing

https://doi.org/10.1021/acsomega.6c00294
ACS Omega 2026, 11, 35326−35336

amounts of art-*Ab*Lys1 (10−60 μg per disk) were applied to bacterial lawns, and inhibition zone diameters were measured after incubation. The radius of the inhibition zone (r) was calculated from the measured diameter, and the square of the radius (r^2) was plotted against the natural logarithm of the applied antimicrobial quantity (ln Q). Linear regression analysis was performed using GraphPad Prism 8. The MIC value was estimated from the regression parameters according to $r^2 = a \cdot \ln(Q) + b$; $\ln(\text{MIC}) = -b/a$; $\text{MIC} = e^{(-b/a)}$. Only data points producing measurable inhibition zones were included in the regression analysis.

Bioinformatics and Structure Analysis. The structure of art-*Ab*Lys1 was predicted using AlphaFold2.[41,42] Chimera was used to inspect the models and crystal structures.[43] The N-terminal amino acid sequence of the purified art-*Ab*Lys1 protein was determined by manual Edman degradation. The released phenylthiohydantoin (PTH)−amino acids were identified by thin-layer chromatography (TLC), as previously described.[44]

Cytotoxicity Assay in Human Cells. The cytotoxicity of art-*Ab*Lys1 was evaluated using a standard MTT cell viability assay. The human colorectal adenocarcinoma cell line Caco-2 (ATCC HTB-37) was cultured in Dulbecco's modified Eagle medium (DMEM) supplemented with 10% fetal bovine serum (FBS), 1% penicillin−streptomycin, and 1% nonessential amino acids (NEAA). Cells were maintained at 37 °C in a humidified incubator with 5% CO_2. For the assay, Caco-2 cells were seeded in 96-well plates at a density of 1×10^4 cells per well and allowed to attach overnight. Cells were then exposed to different concentrations of art-*Ab*Lys1 (0−100 μg/mL) for 24 or 48 h. Following treatment, MTT solution (5 mg/mL) was added and plates were incubated for 2 h at 37 °C. The resulting formazan crystals were dissolved in DMSO, and absorbance was measured at 560 nm using an Infinite 200 PRO microplate reader (Tecan, Switzerland). Cell viability was calculated as

$$\text{Cell viability (\%)} = (\text{absorbance\_sample}/\text{absorbance\_control}) \times 100$$

Experiments were performed in duplicate and repeated in three independent biological replicates. Results are presented as the mean ± standard deviation.

Encapsulation of Art-*Ab*Lys1 in Sodium Alginate Particles. To 8 mL of sodium alginate solution (1.5% w/v), 2 mL of the purified enzyme was added. The solution (10 mL, 1.053 mg/mL enzyme) was dispensed dropwise into 10 mL of a calcium chloride solution (100 mM) at a controlled flow rate of 2 mL/min with a predefined particle size of 300 μm (Encapsulator B390; Buchi Corporation, USA). The resulting beads were collected and washed thoroughly with double-distilled water (ddH_2O). The calcium chloride solution was retained, and the protein concentration was determined using the Bradford assay to calculate the percentage of enzyme encapsulation. To assess the antimicrobial activity of the formulated particles, a turbidity assay was performed using lytic activity against inactivated *A. baumannii* cells as the substrate.

Antibacterial Activity against Biofilms Formed by Pathogenic Bacteria. Crystal violet staining was employed to evaluate antibacterial activity, following the protocol of Wilson et al. (2017),[45] with some modifications. Initially, 20 μL of the overnight culture of each bacterium was added to 2 mL of LB nutrient medium in a 12-well microplate and incubated at 37 °C for 48 h to allow for biofilm formation at the bottom of each well. Once the biofilm was formed, the supernatant medium was removed by washing, and either the free enzyme art-*Ab*Lys1 or the immobilized art-*Ab*Lys1-Alg-Ps system was added to the wells along with LB medium to a final volume of 2 mL. The microplate was then incubated at 37 °C for 24 h to enable the enzyme formulations to act on the biofilms. The following day, the supernatant was discarded and the microplate was left to dry at 37 °C. Subsequently, 600 μL crystal violet solution (0.1% w/v in ethanol) was added to each well and incubated at room temperature for 20 min. Afterward, the wells were washed with ddH_2O and dried at 37 °C for 20 min. Finally, 1.5 mL of 30% acetic acid solution was added, and the absorbance was measured at 585 nm. As a control, free art-*Ab*Lys1 (5 μM) and sodium alginate particles without enzyme encapsulation were used.

Statistical Analysis. All experiments were performed in at least three independent biological replicates with technical duplicates. Data are presented as mean ± standard deviation. Statistical comparisons between two groups were performed using Student's t-test, while comparisons among multiple groups were analyzed using one-way ANOVA followed by Tukey's multiple comparison test. Differences were considered statistically significant at $p < 0.05$.

RESULTS AND DISCUSSION

Design and Fusion of *Ab*Lys1 with AMP for the Generation of Art-*Ab*Lys1

Fusion of endolysins with antimicrobial peptides has been proposed as a strategy to enhance activity against Gram-negative bacteria.[17,46,47] A previous study[35] established that the N-terminus of *Ab*Lys1 adopts an antenna-like structure that contains a short sequence with predicted antimicrobial activity that destabilizes the outer membrane of *A. baumannii*, thus providing access of the catalytic domain of *Ab*Lys1 to the peptidoglycan (Figure 1A). In the present study, we aimed to enhance the antimicrobial activity of the antenna-like structure by fusing a short AMP at the N-terminus of *Ab*Lys1.

The cysteine-functionalized decapeptide CLLKKLLKKC has been found to effectively eradicate Gram-negative carbapenem-resistant clinical isolates of *A. baumannii* and other bacteria both in vitro and in vivo.[20,21] For example, the (MIC) of the peptide against 20 clinical isolates of carbapenem-resistant *A. baumannii* was found lower than or equal to 63.1 μM. The peptide belongs to the family of α-helical AMPs with the general sequence $(XXYY)_n$, where X is a hydrophobic amino acid, Y is a cationic amino acid, and n is the number of repeat units.[20,21] Previous studies[20,21] have revealed that $(LLKK)_3$ has an optimum composition and structure. The incorporation of Cys residues at the termini of $(LLKK)_n$ peptides (n = 2, 3) was demonstrated to broaden the antimicrobial spectrum of the peptides toward a range of Gram-negative bacteria.

Structure prediction of art-*Ab*Lys1 using the AlphaFold2 server[41] generated five models with high confidence (the pLDDT for each of these five models was 90.8, 89.4, 91, 92.1, and 92.6). Figure 1B shows the predicted structure of art-*Ab*Lys1 with different possible AMP conformations at the N-terminal end of art-*Ab*Lys1. An α-helical conformation for AMP was formed in four of the five structures. A structural superposition of the best-predicted AF2 model onto the crystal structure of *Ab*Lys1 (PDB id 8APP) is shown in Figure 1C. In all predicted models, AMP is neither buried nor sterically hindered and adopts an extended conformation, protruding from the N-terminal domain of the protein. This conformation allows unrestricted interaction/binding with the outer membrane of Gram-negative bacteria, allowing access of the catalytic C-terminal domain to the peptidoglycan. Moreover, the presence of the AMP extension increases the positive surface charges of the N-terminal domain as shown by electrostatic surface analysis (Figure 1D). Notably, the predicted models also showed that the N-terminal domain can adopt different orientations, thus allowing more flexibility in interactions with the bacterial membrane for optimal binding. This is in agreement with the different orientations of the N-terminal domain observed in the crystal structure of *Ab*Lys1 for each of the four *Ab*Lys1 molecules in the crystallographic asymmetric unit.[35]

Biochemical Characterization of Art-*Ab*Lys1

The engineered enzyme art-*Ab*Lys1 was created by PCR, cloned, and expressed in *E. coli* BL21(DE3) as a 6His-tagged protein. The 6×His tag enabled art-*Ab*Lys1 to be effectively purified by immobilized metal ion affinity chromatography on a Ni^{2+}-IDA-Sepharose column (Figure 2). The identity of the purified art-*Ab*Lys1 protein was confirmed by N-terminal amino acid sequence analysis. The obtained N-terminal sequence was consistent with the predicted sequence of the recombinant protein (Met−Cys−Leu−Leu−Lys), confirming correct expression of the engineered construct. In addition, the recombinant enzyme bound to the Ni^{2+}-IDA affinity column via its C-terminal

https://doi.org/10.1021/acsomega.6c00294
ACS Omega 2026, 11, 35326−35336

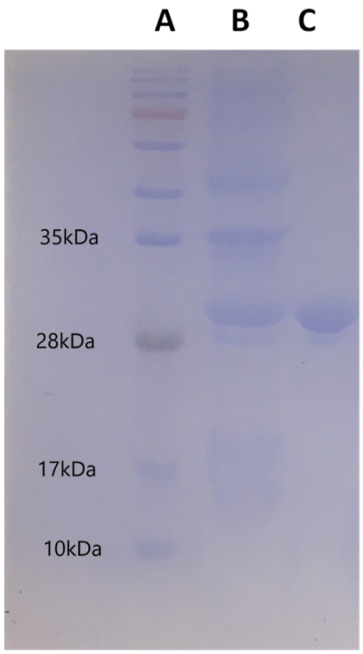

Figure 2. SDS-PAGE analysis of art-*Ab*Lys1 purification using immobilized metal affinity chromatography. Protein bands were stained with Coomassie Brilliant Blue R-250. Lane A, protein ladder. Lane B, *E. coli* BL21 (DE3) crude extract after induction with IPTG (1 mM); Lane C, art-*Ab*Lys1 purified by affinity chromatography on Ni^{2+}-IDA-Sepharose. Lane C depicts the fraction eluted by 250 mM imidazole.

His_6-tag and migrated at the expected molecular weight on SDS-PAGE (Figure 2), confirming the integrity of the expressed protein.

The subsequent step involved comparative evaluation of the biochemical properties and lytic activity of art-*Ab*Lys1 relative to wild-type *Ab*Lys1. The activity of both enzymes was determined by employing turbidity assays and measuring the time-dependent turbidity changes of a Remazol Brilliant Blue-R-labeled peptidoglycan (RBBR-PNG) suspension (Figure 3A), and inactivated *A. baumannii* cell suspensions (Figure 3B). As shown in Figure 3A,B, art-*Ab*Lys1 displayed enhanced activity toward RBBR-PNG and *A. baumannii* cells compared to the wild-type enzyme *Ab*Lys1. For example, the apparent rate constants for RBBR-PNG degradation (Figure 3A) were determined to be 0.298 ± 0.028 min^{-1} (n = 3) for *Ab*Lys1 and 0.729 ± 0.139 min^{-1} (n = 3) for art-*Ab*Lys1, corresponding to an approximately 2.4-fold increase in activity for art-*Ab*Lys1. From the data shown in Figure 3B, the apparent rate constants for the time-dependent decrease in turbidity in *A. baumannii* cells were determined to be 0.003 ± 0.001 min^{-1} (n = 3) for *Ab*Lys1 and 0.022 ± 0.001 min^{-1} (n = 3) for art-*Ab*Lys1, indicating that art-*Ab*Lys1 exhibits an approximately 7.6-fold enhancement in activity relative to *Ab*Lys1.

Statistical comparison of the calculated apparent rate constants confirmed that the differences between *Ab*Lys1 and art-*Ab*Lys1 were statistically significant (Student's t-test, $p < 0.05$). The greater enhancement of art-*Ab*Lys1 activity against intact cells compared to its activity against isolated peptidoglycan supports the hypothesis that fusion of the decapeptide to *Ab*Lys1 improves the access of the catalytic domain to the peptidoglycan layer. Although the precise mechanism was not directly investigated in this study, antimicrobial peptides are known to interact with bacterial membranes and have been used in previous studies to enhance the activity of engineered endolysins against Gram-negative bacteria.[17−19]

The structural stability/integrity of art-*Ab*Lys1 was investigated using differential scanning calorimetry (DSF), as previously described for the wild-type enzyme.[35] As shown in Figure 4, fusion of the AMP

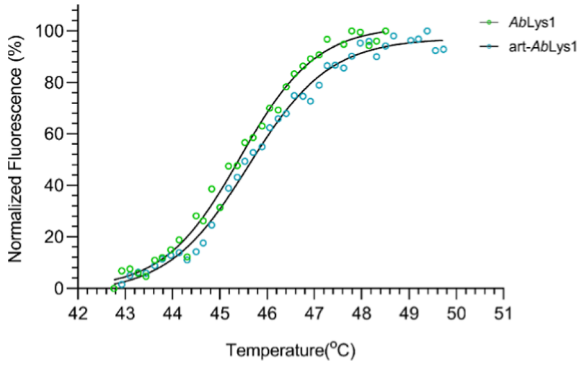

Figure 4. Thermal stability of *Ab*Lys1 and art-*Ab*Lys1. Melting curves of art-*Ab*Lys1 and *Ab*Lys1 for the determination of melting temperatures (T_m). The T_m was determined to be 45.43 ± 0.07 °C (R^2 0.9935) and 45.61 ± 0.11 °C (R^2 0.9922) for the *Ab*Lys1 and art-*Ab*Lys1, respectively.

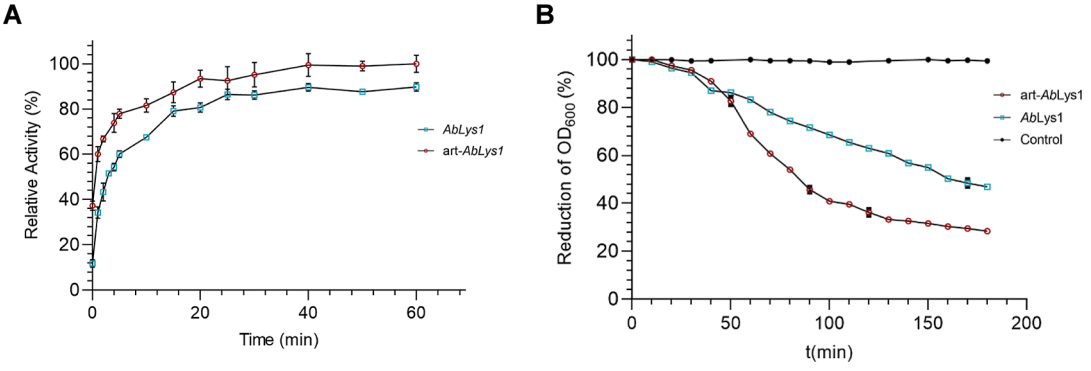

Figure 3. Comparison of *Ab*Lys1 and art-*Ab*Lys1 activity. (A) The enzymatic activity of art-*Ab*Lys1 and the wild-type *Ab*Lys1 (150 μg) was assessed by monitoring the time-dependent increase in absorbance using as substrate dye-labeled Remazol Brilliant Blue-R peptidoglycan isolated from *A. baumannii* (RBBR-PNG). Absorbance changes were recorded at 595 nm at regular time intervals under fixed conditions (25 °C). The assay was conducted using purified art-*Ab*Lys1 (○) or the wild-type *Ab*Lys1 (□). The relative activity (%) is defined as the maximum increase in final optical density at 595 nm upon completion of the enzymatic reaction. (B) The enzymatic activity of art-*Ab*Lys1 and *Ab*Lys1 was assessed by measuring time-dependent turbidity changes in a suspension of *A. baumannii* cells. Turbidity was monitored spectrophotometrically at 600 nm at regular time intervals under fixed conditions (25 °C), using art-*Ab*Lys1 (○) or the wild-type *Ab*Lys1 (□). Reaction without the enzyme (●) served as control. Data are presented as mean ± SD from three independent experiments (n = 3). Statistical significance was evaluated using Student's t-test ($p < 0.05$).

https://doi.org/10.1021/acsomega.6c00294
ACS Omega 2026, 11, 35326−35336

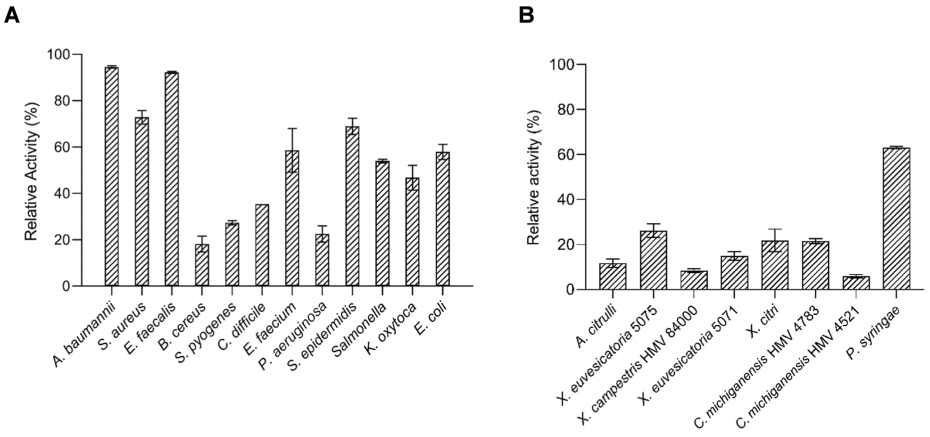

Figure 5. Activity of art-*Ab*lys1 against representative human (A) or plant (B) pathogens. The enzymatic activity of art-*Ab*Lys1 was assessed by monitoring time-dependent turbidity changes in bacterial cell suspensions. Turbidity was measured spectrophotometrically at 600 nm under fixed conditions (25 °C) using purified art-*Ab*Lys1. Relative activity (%) was calculated after subtraction of the background signal obtained from control reactions without enzyme. The corrected activity was normalized to the maximum activity observed in the assay and is defined as 100%. Data represent mean ± SD from three independent experiments (n = 3).

decapeptide at the N-terminal of *Ab*Lys1 did not affect the thermal stability of art-*Ab*Lys1. The melting temperatures (T_m) were 45.6 ± 0.1 °C and 45.4 ± 0.1 °C for art-*Ab*Lys1 and *Ab*Lys1, respectively. This indicates that the engineering strategy adopted in the present study did not affect or compromise the stability of the enzyme.

Antimicrobial Activity of Art-*Ab*Lys1

A previous study[35] showed that *Ab*Lys1 exhibits significant antimicrobial activity against *A. baumannii* and low antimicrobial activity (approximately 10% of that against *A. baumannii*) against other microbial pathogens such as *Enterococcus faecalis*, *S. aureus*, *Streptococcus pyogenes*, *Bacillus cereus*, and *Clostridioides difficile*. This indicated that *Ab*Lys1 possesses high specificity and a pronounced preference for its native host, consistent with its origin as an endolysin encoded by *Acinetobacter* phage TZA1.[48] In addition to these bacterial strains, the following strains were also evaluated: clinically isolated *E. faecium*, *Salmonella*, *K. oxytoca* and *S. epidermidis*, the commercially available *P. aeruginosa* ATCC 27853, and *E. coli* DH5α. Figure 5A depicts the lytic activity of art-*Ab*Lys1 toward the collection of 12 different human pathogens. The results showed that art-*Ab*Lys1 exhibited lytic activity against several tested bacterial strains, with variable levels of activity across species. The highest activity was observed against *E. faecium*, *S. epidermidis*, and *E. coli* DH5α.

Furthermore, Art-*Ab*Lys1 was tested for lytic activity against a range of phytopathogenic bacteria. In an ongoing effort to develop alternative strategies for the protection of plants against bacterial diseases, endolysins represent a promising but underexplored class of antimicrobials in plant protection strategies.[6,49,50] The lytic activity of art-*Ab*Lys1 against eight bacterial strains was evaluated (Figure 5B). Among the strains tested, *P. syringae* exhibited the highest susceptibility, with an activity level of 63.2%. This was followed by *X. euvesicatoria* 5075 (26.1%), *X. citri* (21.1%), and *X. euvesicatoria* 5071 (15.0%). In contrast, *Ab*Lys1 displayed <5% of the measured art-*Ab*Lys1 activity toward plant pathogens. The observed variation in susceptibility among the tested strains highlights the efficacy of art-*Ab*Lys1 and further suggests that art-*Ab*Lys1 displays lytic activity against several strains, although with varying degrees of effectiveness. These findings support the potential application of art-*Ab*Lys1 as a biocontrol agent in agriculture, especially against high-impact pathogens, such as *P. syringae*.

Taken together, the turbidimetric data demonstrated altered substrate specificity, expanded strain coverage, and improved lytic performance against both Gram-positive and Gram-negative bacteria. These results suggest that the fused AMP contributes to improved access of the catalytic domain to the peptidoglycan layer. As predicted (Figure 1B), the exposed AMP structure at the N-terminal domain allows for its interaction with the bacterial membrane, enhancing enzymatic access to peptidoglycan substrates. This structural adaptation likely contributes to the expanded lytic spectrum of art-*Ab*Lys1 compared to its wild-type counterpart.

The antimicrobial activity of art-*Ab*Lys1 toward human pathogens (*E. faecium*, *A. baumannii*, *K. oxytoca*, *S. aureus*, *P. aeruginosa* and *E. coli* DH5α) was further assessed using the Disk Diffusion Method. The amount of art-*Ab*Lys1 used ranged from 10 μg to 60 μg. As shown in Figure 6, clear zones of bacterial growth inhibition were observed for all tested strains, although with varying inhibition activities, as reflected by the different zone diameters. For example, clear growth inhibition zones were visible around all art-*Ab*Lys1 concentrations in *S. aureus* and *A. baumannii*. For *E. faecium*, clear growth inhibition zones were observed around the disks containing 20, 40, and 60 μg of art-*Ab*Lys1. For *K. oxytoca* and *E. coli* DH5α, inhibition was achieved with 15 to 60 μg of art-*Ab*Lys1. A lower activity was observed against *P. aeruginosa*, where zones were detected only at 40 and 60 μg of art-*Ab*Lys1. These results demonstrate that the antimicrobial activity of art-*Ab*Lys1 against a variety of bacterial strains is concentration- and strain-dependent, similar to that exhibited by antibiotics.

Linear regression analysis of r^2 versus ln(Q) showed strong correlations for several bacterial strains, with R^2 values ranging from 0.91 to 0.98 (Figure S1). The estimated MIC values are presented in Table S1. These results suggest that art-*Ab*Lys1 exhibits antimicrobial activity in the low μg range against the tested bacterial strains under the conditions examined.

The antibacterial activity observed for art-*Ab*Lys1 in the present study is comparable to that of previously reported endolysins, which exhibit measurable inhibition zones in agar diffusion assays and MIC values in the low μg/mL range. For example, the endolysin LysAB1245 demonstrated MIC values between 4.68 and 9.36 μg/mL against several clinically relevant pathogens, including *A. baumannii* and *P. aeruginosa*.[51] In another study, the engineered fusion endolysin (lysAB-vT2-fusion) exhibited a MIC of approximately 2 mg/mL against *A. baumannii*, whereas the native enzyme showed significantly lower activity (MIC > 10 mg/mL).[52]

Cytotoxicity of Art-*Ab*Lys1 in Caco-2 Cells

The cytotoxicity of art-*Ab*Lys1 toward human Caco-2 cells was evaluated using an MTT assay following 24 and 48 h of exposure (Figure S2). At concentrations up to 25 μg/mL, cell viability remained close to control levels after 24 h incubation, indicating minimal cytotoxic effects. A moderate decrease in viability was observed at 50 μg/mL, while a pronounced reduction occurred only at the highest tested concentration (100 μg/mL). A similar trend was observed after 48 h exposure. Cell viability remained above 90% at concentrations up to 10 μg/mL and gradually decreased at higher

https://doi.org/10.1021/acsomega.6c00294
ACS Omega 2026, 11, 35326−35336

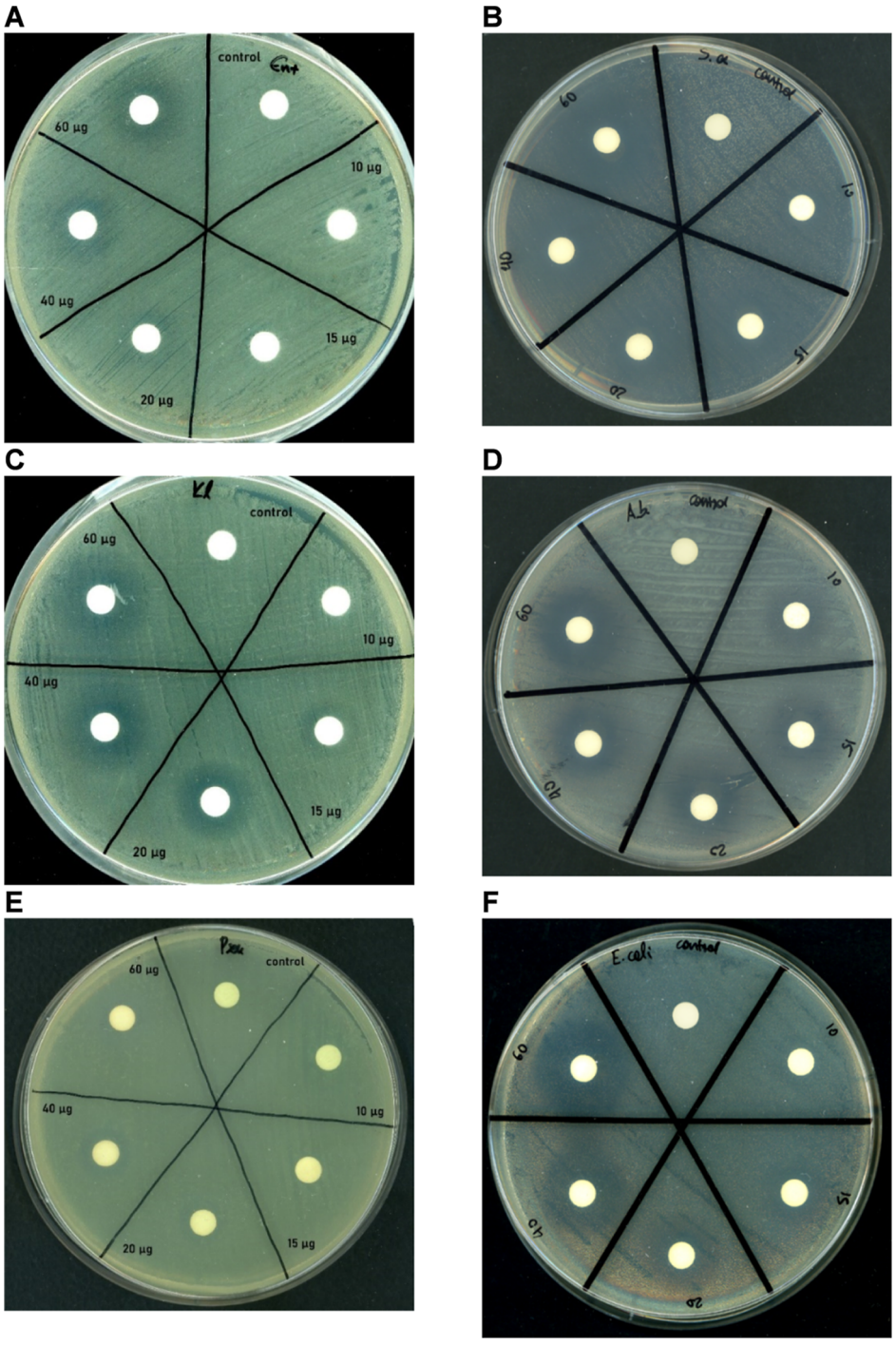

Figure 6. Agar disk diffusion assay of art-*Ab*Lys1 (0−60 μg). The antibacterial activity of art-*Ab*Lys1 was evaluated using the agar disk diffusion method against clinically isolated bacterial strains (A) *E. faecium*, (B) *S. aureus* (MSSA) ATCC 25923, (C) *K. oxytoca*, (D) *A. baumannii*, (E) *P. aeruginosa* ATCC 27853 and (F) the laboratory strain *E. coli* DH5α.

concentrations. The concentrations corresponding to the estimated antimicrobial MIC values (approximately 3−6 μg/mL) did not significantly affect Caco-2 cell viability. These results indicate that the antimicrobial activity occurs at concentrations well below those causing cytotoxic effects, suggesting a favorable therapeutic window. Overall, the results demonstrate that art-*Ab*Lys1 exhibits low cytotoxicity toward human cells, with significant reductions in viability occurring only at concentrations substantially higher than those required for antimicrobial activity. These findings are consistent with previous studies[53] showing that bacteriophage endolysins generally exhibit low toxicity toward eukaryotic cells, as their catalytic activity specifically targets bacterial peptidoglycan, which is absent in mammalian and plant cells. Although plant cell models were not included in the present study, evaluation of plant cell compatibility will be investigated in future studies.

Encapsulation of Art-*Ab*Lys1 in Alginate Beads and Characterization

Previous studies have demonstrated that endolysins exhibit a strong safety profile in topical and systemic administration in murine models.[54] However, the susceptibility of endolysins to environmental conditions results in the rapid denaturation of the enzyme, and the limited in vivo half-life of endolysins presents significant challenges for therapeutic development. To overcome these limitations, we

https://doi.org/10.1021/acsomega.6c00294
ACS Omega 2026, 11, 35326−35336

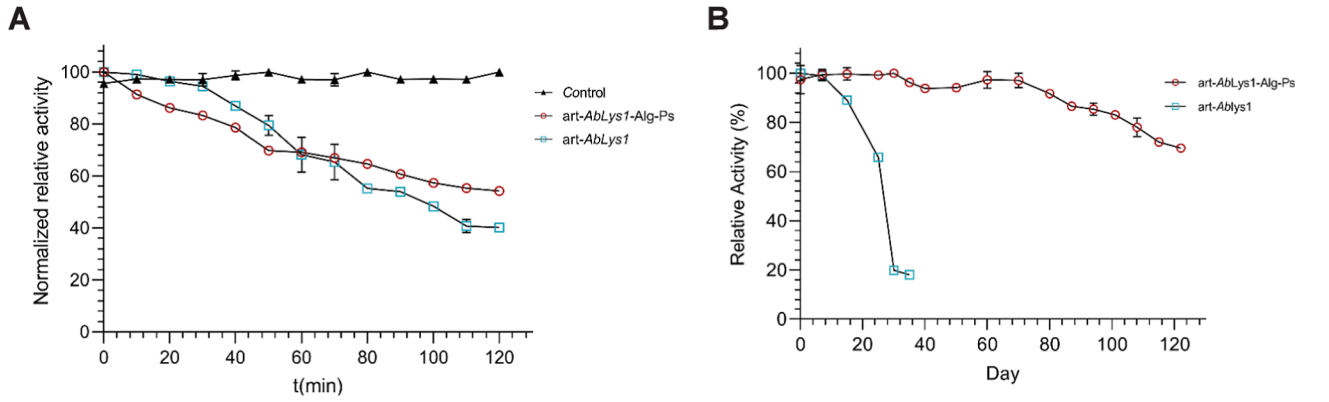

Figure 7. Enzymatic activity of art-*Ab*Lys1 and art-*Ab*Lys1-Alg-Ps assessed by time-dependent turbidity changes in a suspension of *A. baumannii* cells. Turbidity was monitored spectrophotometrically at 600 nm at regular time intervals under fixed conditions (25 °C), using art-*Ab*Lys1 (□), or art-*Ab*Lys1-Alg-Ps (○). Reaction without the enzyme (▲) served as control. (B) Time course of operational stability of art-*Ab*Lys1 and art-*Ab*Lys1-Alg-Ps. The enzymatic activity of art-*Ab*Lys1 or art-*Ab*Lys1-Alg-Ps was assessed by measuring time-dependent turbidity changes in a suspension of *A. baumannii* cells. Turbidity was monitored spectrophotometrically at 600 nm at regular time intervals under fixed conditions (25 °C), using art-*Ab*Lys1 (□) or art-*Ab*Lys1-Alg-Ps (○). Data are presented as mean ± SD from three independent experiments (n = 3). Statistical significance was evaluated using Student's t-test ($p < 0.05$).

employed an encapsulation strategy, in which art-*Ab*Lys1 was incorporated into sodium alginate beads. Encapsulation of purified art-*Ab*Lys1 was achieved using calcium alginate beads (art-*Ab*Lys1-Alg), with an encapsulation efficiency of 93%. The lytic activity of art-*Ab*Lys1-Alg against inactivated *A. baumannii* was assessed using a turbidity assay. In Figure 7A, the apparent rate constant for the time-dependent turbidity changes of *A. baumannii* cells induced by art-*Ab*Lys1-Alg-Ps was determined to be 0.011 ± 0.001 min^{-1} (n = 3). Statistical comparison of the calculated rate constants confirmed a significant difference between the free and encapsulated enzyme (Student's t-test, $p < 0.05$). The results confirmed that the encapsulated enzyme retained its lytic activity, albeit with approximately 20% lower efficiency than that of the free enzyme.

The operational stability of both free and encapsulated enzymes was evaluated using a turbidity assay over a period of 120 days. As illustrated in Figure 7B, the encapsulated enzyme demonstrated substantially enhanced stability compared with that of the free enzyme. The free enzyme retained approximately 50% of its initial activity within the first 25 days; however, it was almost completely inactivated by day 40. In contrast, art-*Ab*Lys1-Alg maintained nearly full lytic activity for approximately 80 days and retained approximately 70% of its activity by day 122. These findings indicate that the encapsulation of art-*Ab*Lys1 in sodium alginate beads significantly enhanced enzymatic stability and enabled enzyme reuse, thereby improving the cost efficiency and sustainability of the method.

The enhanced antibiofilm activity observed for the alginate-encapsulated enzyme may reflect prolonged exposure of the biofilm to the enzyme rather than a direct increase in its intrinsic catalytic activity. Alginate matrices are known to provide a protective microenvironment and can enable sustained release of encapsulated proteins.[22,28,29] Therefore, the improved antibiofilm performance of art-*Ab*Lys1-Alg likely results from a combination of increased stability and prolonged availability of the enzyme at the biofilm interface. Kaur et al. (2020)[22] developed alginate−chitosan nanoparticles loaded with the endolysin LysMR-5, demonstrating improved stability and sustained antibacterial activity against multidrug-resistant *S. aureus* and *S. epidermidis* strains. Similarly, Yao et al. (2021)[55] formulated an alginate hydrogel encapsulating the chimeric lysin ClyC, which provided sustained release and continuous antibacterial effects against *S. aureus*, showing promise in treating osteomyelitis in a mouse model.

Antibiofilm Activity of Art-*Ab*Lys1-Alg Beads

The antibiofilm activity of art-*Ab*Lys1-Alg beads was evaluated against selected Gram-negative bacteria. Figure 8 shows the results of the biofilm degradation assay, illustrating the efficacy of free and encapsulated art-*Ab*Lys1 in disrupting biofilms formed by *P. aeruginosa* ATCC 27853 and the clinically isolated strains *A. baumannii* and *Streptococcus pneumoniae*. The extent of biofilm degradation was quantified based on the reduction in optical density at 585 nm (OD_{585}), indicating the decrease in adherent biomass. The control groups (untreated biofilms) exhibited the highest OD values across all bacterial species, confirming the robustness of biofilm formation.

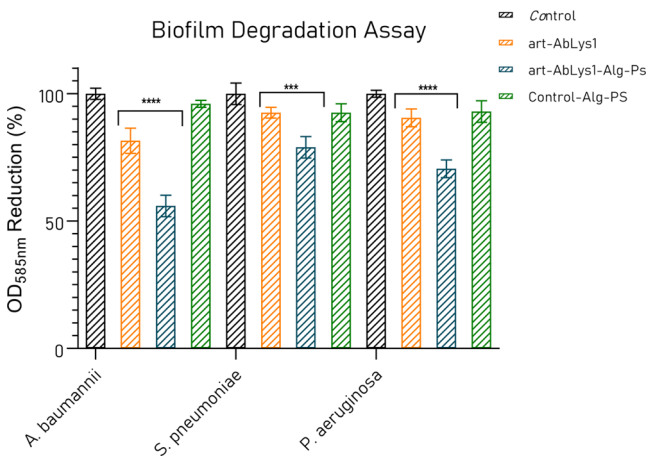

Figure 8. Antibiofilm activity of the art-*Ab*Lys1-Alg-Ps, art-*Ab*Lys1, and alginate beads (Alg-PS) without encapsulated enzyme against bacterial biofilms as a control. The biofilm-disrupting activity of the art-*Ab*Lys1-Alg-Ps was evaluated in comparison to the free enzyme art-*Ab*Lys1 and the control alginate beads (Alg-PS). The assay was conducted against biofilms formed by *A. baumannii*, *P. aeruginosa* ATCC 27853, and *S. pneumoniae*. Data represent mean ± SD from three independent experiments (n = 3). Statistical significance was evaluated using one-way ANOVA followed by Tukey's multiple comparison test.

The antibiofilm activity of the free enzyme (art-*Ab*Lys1), the encapsulated enzyme (art-*Ab*Lys1-Alg-PS), and the corresponding controls was evaluated against *A. baumannii*, *S. pneumoniae*, and *P. aeruginosa*. Statistical analysis was performed using one-way ANOVA followed by Tukey's multiple comparison test. Treatment with free art-*Ab*Lys1 (orange bars) led to a significant reduction in biofilm mass, particularly in *A. baumannii*, where degradation reached 18.5%. However, the encapsulated form, art-*Ab*Lys1-Alg-Ps, demonstrated superior biofilm degradation, especially against *A. baumannii*, with a reduction of approximately 44 ± 3% (difference 25.5%, $p < 0.0001$).

https://doi.org/10.1021/acsomega.6c00294
ACS Omega 2026, 11, 35326−35336

In the case of *S. pneumoniae*, art-*Ab*Lys1-Alg-Ps also exhibited improved biofilm degradation (21 ± 3%) compared to free art-*Ab*Lys1, although to a lesser extent, with a reduction of approximately 7.5% relative to the free enzyme (difference 13.5%, $p = 0.0009$). Biofilm degradation in *P. aeruginosa* ATCC 27853 followed a similar trend, with the encapsulated enzyme demonstrating enhanced efficacy (30.0 ± 2.5%) over the free enzyme (9.5%), although the reduction remained lower than that observed for *A. baumannii* (difference 20%, $p < 0.0001$). In all cases, the control-alginate beads did not significantly affect biofilm integrity, confirming that the antibiofilm activity was due to the enzymatic activity of art-*Ab*Lys1 ($p > 0.2$ in all cases). These results indicate that encapsulation in sodium alginate enhances the antibiofilm efficacy of art-*Ab*Lys1, potentially due to improved enzyme stability and prolonged activity. These findings highlight the potential of art-*Ab*Lys1-Alg-Ps as an effective antibiofilm strategy, particularly against *A. baumannii*, a major pathogen associated with biofilm-related infections.

CONCLUSIONS

The present study demonstrates the successful engineering and characterization of an AMP-fused endolysin designed to enhance antibacterial activity against *A. baumannii* and other clinically relevant human and plant pathogens. The engineered enzyme displayed lytic activity against several Gram-positive and Gram-negative human and plant pathogens, although the magnitude of activity varied among the tested strains. Structural predictions revealed that the AMP domain adopts a stable extended conformation, supporting its functional role in membrane destabilization. DSF analysis indicated that the fusion did not compromise protein stability. Furthermore, encapsulation of art-*Ab*Lys1 in alginate beads significantly improved the operational stability of the enzyme. The encapsulated enzyme also demonstrated antibiofilm activity against *A. baumannii*, *S. pneumoniae*, and *P. aeruginosa*, underscoring its potential for applications in antimicrobial coatings and other therapeutic formulations. Alginate encapsulation improved the antibiofilm performance of the enzyme, likely due to enhanced stability and sustained exposure. These findings highlight the potential of art-*Ab*Lys1 as a stable engineered endolysin for antimicrobial applications.

ASSOCIATED CONTENT

Data Availability Statement

The authors declare that the data supporting the findings of this study are available within the paper and in Supporting Information file. Should any raw data files be needed in another format they are available from the corresponding author upon reasonable request.

Supporting Information

The Supporting Information is available free of charge at https://pubs.acs.org/doi/10.1021/acsomega.6c00294.

Figure S1: quantitative estimation of antimicrobial potency based on disk diffusion assays. Figure S2: cytotoxicity assessment of art-*Ab*Lys1 in human Caco-2 cells using an MTT assay. Table S1: estimated minimum inhibitory concentration (MIC) values of art-*Ab*Lys1 against selected bacterial strains (PDF)

AUTHOR INFORMATION

Corresponding Author

Nikolaos E. Labrou − *Laboratory of Enzyme Technology, Department of Biotechnology, School of Applied Biology and Biotechnology, Agricultural University of Athens, Athens GR-11855, Greece; Research and Innovation Center of the Agricultural University of Athens, Institute of Nanobiotechnology, Sustainable Development and Artificial Intelligence, Athens GR-11855, Greece;* orcid.org/0000-0003-1925-9867; Email: Lambrou@aua.gr

Authors

Georgios E. Premetis − *Laboratory of Enzyme Technology, Department of Biotechnology, School of Applied Biology and Biotechnology, Agricultural University of Athens, Athens GR-11855, Greece*

Panagiota Pantiora − *Laboratory of Enzyme Technology, Department of Biotechnology, School of Applied Biology and Biotechnology, Agricultural University of Athens, Athens GR-11855, Greece*

Nirmal Poudel − *Turku Bioscience Centre, University of Turku and Åbo Akademi University, Turku 20521, Finland*

Nikolaos Georgakis − *Laboratory of Enzyme Technology, Department of Biotechnology, School of Applied Biology and Biotechnology, Agricultural University of Athens, Athens GR-11855, Greece*

Eleni Aikaterini Tzanetopoulou − *Laboratory of Enzyme Technology, Department of Biotechnology, School of Applied Biology and Biotechnology, Agricultural University of Athens, Athens GR-11855, Greece*

Anastassios C. Papageorgiou − *Turku Bioscience Centre, University of Turku and Åbo Akademi University, Turku 20521, Finland;* orcid.org/0000-0002-7980-1120

Complete contact information is available at: https://pubs.acs.org/10.1021/acsomega.6c00294

Author Contributions

G.E.P. performed experiments, analyzed data, wrote the manuscript; E.A.T., performed experiments, analyzed data; N.G., P.P., analyzed data, performed experiments; edited manuscript; N.P. performed the molecular modeling and structure analysis; A.C.P. supervised the structural modeling and analysis, edited the manuscript; N.E.L. conceived the project, planned and supervised experiments, wrote the manuscript.

Funding

The research work was supported by the Hellenic Foundation for Research and Innovation (H.F.R.I.) under the third Call for H.F.R.I. Research projects to support Faculty Members and Researchers (Project Number: 26897). N.P. would like to thank Instrumentarium Science Foundation for funding. The open access publishing of this article is financially supported by HEAL-Link.

Notes

The authors declare no competing financial interest.

ACKNOWLEDGMENTS

We thank Angeliki Stathi (Department of Microbiology, "Aghia Sophia" Children's Hospital, Athens, Greece) for her supervision and assistance with the microbiological experiments. The authors gratefully acknowledge Sofia Marka (Agricultural University of Athens) for assistance with the cell culture and MTT experiments. The publication of the article in OA mode was financially supported by HEAL-Link.

■ ABBREVIATIONS

AMP, antimicrobial peptide; art-*Ab*Lys1, engineered *Ab*Lys1 fused with AMP; art-*Ab*Lys1-AlgPs, alginate-encapsulated art-*Ab*Lys1; *Ab*Lys1, endolysin from *A. baumannii* phage *Ab*TZA1; ATCC, American Type Culture Collection; GH24, glycoside hydrolase family 24; MDR, multidrug-resistant; RBBR, Remazol Brilliant Blue-R; RBBR-PNG, RBBR-labeled peptidoglycan; WHO, World Health Organization

■ REFERENCES

(1) Cui, B.; Peng, G.; Wang, L. E.; Deng, Y. Signaling in *Acinetobacter baumannii*: Quorum Sensing and Nucleotide Second Messengers. *Comput. Struct. Biotechnol. J.* **2025**, *27*, 2168−2175.

(2) Ferrara, F.; Martellone, L.; Vaccaro, M.; Coluccia, A.; Scognamiglio, M.; Langella, R.; Zovi, A.; Polito, G. Real-Life Impact of Cefiderocol in Carbapenem-Resistant *Acinetobacter baumannii* Infections (CRAb): A Narrative Review. *Eur. J. Clin. Pharmacol.* **2025**, *81* (9), 1231−1240.

(3) Salleh, M. Z. Addressing Antimicrobial Resistance: Structural Insights into Cefiderocol's Mode of Action and Emerging Resistance Mechanisms. *J. Infect. Public Health* **2025**, *18* (9), 102871.

(4) Briers, Y.; Walmagh, M.; Van Puyenbroeck, V.; Cornelissen, A.; Cenens, W.; Aertsen, A.; Oliveira, H.; Azeredo, J.; Verween, G.; Pirnay, J.-P.; Miller, S.; Volckaert, G.; Lavigne, R. Engineered Endolysin-Based "Artilysins" to Combat Multidrug-Resistant Gram-Negative Pathogens. *mBio* **2014**, *5* (4), e01379−14.

(5) Gerstmans, H.; Rodríguez-Rubio, L.; Lavigne, R.; Briers, Y. From Endolysins to Artilysins: Novel Enzyme-Based Approaches to Kill Drug-Resistant Bacteria. *Biochem. Soc. Trans.* **2016**, *44* (1), 123−128.

(6) Vázquez, R.; Gutiérrez, D.; Criel, B.; Dezutter, Z.; Briers, Y. Diversity, Structure−Function Relationships, and Evolution of Cell Wall-Binding Domains of Staphylococcal Phage Endolysins. *Int. J. Biol. Macromol.* **2025**, *310* (Pt 2), 143093.

(7) Warring, S. L.; Sisson, H. M.; Randall, G.; Grimon, D.; Dams, D.; Gutiérrez, D.; Fellner, M.; Fagerlund, R. D.; Briers, Y.; Jackson, S. A.; Fineran, P. C. Engineering an Antimicrobial Chimeric Endolysin That Targets the Phytopathogen *Pseudomonas syringae* pv. *actinidiae*. *J. Biol. Chem.* **2025**, *301* (6), 110224.

(8) Zhang, P.; Zeng, P.; Lai, C. K. C.; Ip, M.; To, K. K. W.; Zuo, Z.; Xia, J.; Leung, S. S. Y. Synergism of Colistin and Globular Endolysins against Multidrug-Resistant Gram-Negative Bacteria. *Int. J. Biol. Macromol.* **2024**, *278* (Pt 2), 134670.

(9) Kocot, A. M.; Briers, Y.; Plotka, M. Phages and Engineered Lysins as an Effective Tool to Combat Gram-Negative Foodborne Pathogens. *Compr. Rev. Food Sci. Food Saf.* **2023**, *22* (3), 2235−2266.

(10) Dams, D.; Pas, C.; Latka, A.; Drulis-Kawa, Z.; Fieseler, L.; Briers, Y. A VersaTile Approach to Reprogram the Specificity of the R2-Type Tailocin toward Different Serotypes of *Escherichia coli* and *Klebsiella pneumoniae*. *Antibiotics* **2025**, *14* (1), 104.

(11) Chiusaroli, L.; Tripiciano, C.; Liberati, C.; De Pieri, M.; Brigadoi, G.; Donà, D. Tackling Multidrug-Resistant Gram-Negative Infections in Children Globally: Current Therapeutic Options and Perspectives. *Expert Opin. Pharmacother.* **2025**, *26* (10), 1205−1220.

(12) Huan, Y.; Kong, Q.; Mou, H.; Yi, H. Antimicrobial Peptides: Classification, Design, Application, and Research Progress in Multiple Fields. *Front. Microbiol.* **2020**, *11*, 582779.

(13) Davani-Davari, D.; Tiwari, R. K.; Parang, K. Future Applications of Cyclic Antimicrobial Peptides in Drug Delivery. *Expert Opin. Drug Delivery* **2025**, *22* (3), 383−404.

(14) Yang, A.; Bai, Y.; Zhang, Y.; Xiao, R.; Zhang, H.; Chen, F.; Zeng, W. Detection and Treatment with Peptide Power: A New Weapon against Bacterial Biofilms. *ACS Biomater. Sci. Eng.* **2025**, *11* (2), 806−819.

(15) Amod, A.; Anand, A. A.; Sahoo, A. K.; Samanta, S. K. Diagnostic and Therapeutic Strategies in Combating Implanted Medical Device-Associated Bacterial Biofilm Infections. *Folia Microbiol.* **2025**, *70* (2), 321−342.

(16) Varotsou, C.; Premetis, G. E.; Labrou, N. E. Characterization and Engineering Studies of a New Endolysin from the *Propionibacterium acnes* Bacteriophage PAC1 for the Development of a Broad-Spectrum Artilysin with Altered Specificity. *Int. J. Mol. Sci.* **2023**, *24* (10), 8523.

(17) Lim, J.; Myung, H.; Lim, D.; Song, M. Antimicrobial Peptide Thanatin-Fused Endolysin PA90 (Tha-PA90) for the Control of *Acinetobacter baumannii* Infection in a Mouse Model. *J. Biomed. Sci.* **2024**, *31* (1), 36.

(18) Luo, Y.; Song, Y. Mechanism of Antimicrobial Peptides: Antimicrobial, Anti-Inflammatory, and Antibiofilm Activities. *Int. J. Mol. Sci.* **2021**, *22* (21), 11401.

(19) Gani, Z.; Kumar, A.; Raje, M.; Raje, C. I. Antimicrobial Peptides: An Alternative Strategy to Combat Antimicrobial Resistance. *Drug Discovery Today* **2025**, *30* (2), 104305.

(20) Wiradharma, N.; Khan, M.; Yong, L. K.; Hauser, C. A. E.; Seow, S. V.; Zhang, S.; Yang, Y. Y. Effect of Thiol Functional Group Incorporation into Cationic Helical Peptides on Antimicrobial Activities and Spectra. *Biomaterials* **2011**, *32* (34), 9100−9108.

(21) Wiradharma, N.; Khoe, U.; Hauser, C. A. E.; Seow, S. V.; Zhang, S.; Yang, Y. Y. Synthetic Cationic Amphiphilic α-Helical Peptides as Antimicrobial Agents. *Biomaterials* **2011**, *32* (8), 2204−2212.

(22) Kaur, J.; Kour, A.; Panda, J. J.; Harjai, K.; Chhibber, S. Exploring Endolysin-Loaded Alginate−Chitosan Nanoparticles as a Future Remedy for Staphylococcal Infections. *AAPS PharmSciTech* **2020**, *21* (6), 233.

(23) Karim, A.; Rehman, A.; Feng, J.; Noreen, A.; Assadpour, E.; Kharazmi, M. S.; Lianfu, Z.; Jafari, S. M. Alginate-Based Nanocarriers for the Delivery and Controlled Release of Bioactive Compounds. *Adv. Colloid Interface Sci.* **2022**, *307*, 102744.

(24) Alrata, L.; Abdulsattar, D.; Madrigal, S.; Pyeatte, S. R.; Zaghloul, M.; Abu-Amer, W.; Arif, B.; Alhamad, T.; Remedi, M.; Lin, Y.; Zayed, M. A. Alginate Formulation for Wound Healing Applications. *Adv. Wound Care* **2025**, *14* (9), 467−478.

(25) Yang, X.; Huang, C.; Wang, H.; Yang, K.; Huang, M.; Zhang, W.; Yu, Q.; Wang, H.; Zhang, L.; Zhao, Y.; Zhu, D. Multifunctional Nanoparticle-Loaded Injectable Alginate Hydrogels with Deep Tumor Penetration for Enhanced Chemo-Immunotherapy of Cancer. *ACS Nano* **2024**, *18* (28), 18604−18621.

(26) Pantakitcharoenkul, J.; Touma, J.; Jovanovic, G.; Coblyn, M. Enzyme-Functionalized Hydrogel Film for Extracorporeal Uric Acid Reduction. *J. Biomed. Mater. Res., Part B* **2024**, *112* (2), No. e35375.

(27) Jiang, Y.; Mi, L.; Xu, X.; Hii, A. R. K.; Wu, Z.; Qi, X. Urease-Catalyzed High-Density Sodium Alginate Microspheres Enable High Oral Bioavailability of Macromolecular Drugs. *Biomater. Sci.* **2024**, *12* (6), 1515−1528.

(28) Ghate, M. M.; Gulati, K.; Poluri, K. M. Alginate Binding Enhances Structural Stability and Potentiates the Lytic Activity of a Bacteriophage Endolysin's Partially Folded Conformation. *Arch. Biochem. Biophys.* **2024**, *760*, 110129.

(29) Vasina, D. V.; Antonova, N. P.; Shidlovskaya, E. V.; Kuznetsova, N. A.; Grishin, A. V.; Akoulina, E. A.; Trusova, E. A.; Lendel, A. M.; Mazunina, E. P.; Kozlova, S. R.; Dudun, A. A.; Bonartsev, A. P.; Lunin, V. G.; Gushchin, V. A. Alginate Gel Encapsulated with an Enzybiotics Cocktail Is Effective against Multispecies Biofilms. *Gels* **2024**, *10* (1), 60.

(30) Xia, Y.; Hu, Z.; Jin, Q.; Chen, Q.; Zhao, C.; Qiang, R.; Xie, Z.; Li, L.; Zhang, H. Structural Characteristics, Functions, and Counteracting Strategies of Biofilms in *Staphylococcus aureus*. *Comput. Struct. Biotechnol. J.* **2025**, *27*, 488−500.

(31) Behera, M.; De, S.; Ghorai, S. M. The Synergistic and Chimeric Mechanism of Bacteriophage Endolysins: Opportunities for Application in Biotherapeutics, Food, and Health Sectors. *Probiotics Antimicrob. Proteins* **2025**, *17* (2), 807−831.

(32) Wang, C.; Zhao, J.; Lin, Y.; Lwin, S. Z. C.; El-Telbany, M.; Masuda, Y.; Honjoh, K. I.; Miyamoto, T. Characterization of Two Novel Endolysins from Bacteriophage PEF1 and Evaluation of Their

https://doi.org/10.1021/acsomega.6c00294
ACS Omega 2026, 11, 35326−35336

Combined Effects on the Control of *Enterococcus faecalis* Planktonic and Biofilm Cells. *Antibiotics* **2024**, *13* (9), 884.
(33) Blanco Massani, M.; To, D.; Meile, S.; Schmelcher, M.; Gintsburg, D.; Coraça-Huber, D. C.; Seybold, A.; Loessner, M. J.; Bernkop-Schnürch, A. Enzyme-Responsive Nanoparticles: Enhancing the Ability of Endolysins to Eradicate *Staphylococcus aureus* Biofilm. *J. Mater. Chem. B* **2024**, *12* (37), 9199−9205.
(34) Hasan, M.; Kim, J.; Liao, X.; Ding, T.; Ahn, J. Antibacterial Activity of Bacteriophage-Encoded Endolysins against Planktonic and Biofilm Cells of Pathogenic *Escherichia coli*. *Microb. Pathog.* **2024**, *193*, 106780.
(35) Premetis, G. E.; Stathi, A.; Papageorgiou, A. C.; Labrou, N. E. Characterization of a Glycoside Hydrolase Endolysin from *Acinetobacter baumannii* Phage AbTZA1 with High Antibacterial Potency and Novel Structural Features. *FEBS J.* **2023**, *290* (8), 2146−2164.
(36) Barry, A. L.; Garcia, F.; Thrupp, L. D. An Improved Single-Disk Method for Testing the Antibiotic Susceptibility of Rapidly Growing Pathogens. *Am. J. Clin. Pathol.* **1970**, *53* (2), 149−158.
(37) Cooper, K. E. Theory of antibiotic inhibition zones in agar media. *Nature* **1955**, *176*, 510−511.
(38) Chandrasekar, V.; Knabel, S. J.; Anantheswaran, R. C. Modeling development of inhibition zones in an agar diffusion bioassay. *Food Sci. Nutr.* **2015**, *3* (5), 394−403.
(39) Hombach, M.; Jetter, M.; Blöchliger, N.; Kolesnik-Goldmann, N.; Keller, P. M.; Böttger, E. C. Rapid disc diffusion antibiotic susceptibility testing for *Pseudomonas aeruginosa, Acinetobacter baumannii* and Enterococcus spp. *J. Antimicrob. Chemother.* **2018**, *73* (2), 385−391.
(40) Asadi, M.; Taheri-Anganeh, M.; Ranjbar, M.; Khatami, S. H.; Maleksabet, A.; Mostafavi-Pour, Z.; Ghasemi, Y.; Keshavarzi, A.; Savardashtaki, A. LYZ2-SH3b as a novel and efficient enzybiotic against methicillin-resistant Staphylococcus aureus. *BMC Microbiol.* **2023**, *23* (1), 257.
(41) Jumper, J.; Evans, R.; Pritzel, A.; Green, T.; Figurnov, M.; Ronneberger, O.; Tunyasuvunakool, K.; Bates, R.; Žídek, A.; Potapenko, A.; Bridgland, A.; Meyer, C.; Kohl, S. A. A.; Ballard, A. J.; Cowie, A.; Romera-Paredes, B.; Nikolov, S.; Jain, R.; Adler, J.; Back, T.; Petersen, S.; Reiman, D.; Clancy, E.; Zielinski, M.; Steinegger, M.; Pacholska, M.; Berghammer, T.; Bodenstein, S.; Silver, D.; Vinyals, O.; Senior, A. W.; Kavukcuoglu, K.; Kohli, P.; Hassabis, D. Highly Accurate Protein Structure Prediction with AlphaFold. *Nature* **2021**, *596* (7873), 583−589.
(42) Mirdita, M.; Schütze, K.; Moriwaki, Y.; Heo, L.; Ovchinnikov, S.; Steinegger, M. ColabFold: Making Protein Folding Accessible to All. *Nat. Methods* **2022**, *19* (6), 679−682.
(43) Pettersen, E. F.; Goddard, T. D.; Huang, C. C.; Couch, G. S.; Greenblatt, D. M.; Meng, E. C.; Ferrin, T. E. UCSF Chimera—A Visualization System for Exploratory Research and Analysis. *J. Comput. Chem.* **2004**, *25* (13), 1605−1612.
(44) Edman, P.; Högfeldt, E.; Sillén, L. G.; Kinell, P. O. Method for Determination of the Amino Acid Sequence in Peptides. *Acta Chem. Scand.* **1950**, *4*, 283−293.
(45) Wilson, C.; Lukowicz, R.; Merchant, S.; Valquier-Flynn, H.; Caballero, J.; Sandoval, J.; Okuom, M.; Huber, C.; Brooks, T. D.; Wilson, E.; Clement, B.; Wentworth, C. D.; Holmes, A. E. Quantitative and Qualitative Assessment Methods for Biofilm Growth: A Mini-Review. *Res. Rev.: J. Eng. Technol.* **2017**, *6* (4), 1−42.
(46) Vander Elst, N.; Bert, J.; Favoreel, H.; Lavigne, R.; Meyer, E.; Briers, Y. Development of Engineered Endolysins with *In Vitro* Intracellular Activity against Streptococcal Bovine Mastitis-Causing Pathogens. *Microb. Biotechnol.* **2023**, *16* (12), 2367−2386.
(47) Chu, D.; Lan, J.; Liang, L.; Xia, K.; Li, L.; Yang, L.; Liu, H.; Zhang, T. Antibacterial Activity of a Novel Highly Thermostable Endolysin, LysKP213, against Gram-Negative Pathogens Is Enhanced When Combined with Outer Membrane-Permeabilizing Agents. *Front. Microbiol.* **2024**, *15*, 1454618.
(48) Nir-Paz, R.; Gelman, D.; Khouri, A.; Sisson, B. M.; Fackler, J.; Alkalay-Oren, S.; Khalifa, L.; Rimon, A.; Yerushalmy, O.; Bader, R.; Amit, S.; Coppenhagen-Glazer, S.; Henry, M.; Quinones, J.; Malagon, F.; Biswas, B.; Moses, A. E.; Merril, G.; Schooley, R. T.; Brownstein, M. J.; Weil, Y. A.; Hazan, R. Successful Treatment of Antibiotic-Resistant Polymicrobial Bone Infection with Bacteriophages and Antibiotics Combination. *Clin. Infect. Dis.* **2019**, *69* (11), 2015−2018.
(49) Zhang, M.; Xu, X.; Lv, L.; Luo, J.; Ahmed, T.; Alsakkaf, W. A. A.; Ali, H. M.; Bi, J.; Yan, C.; Gu, C.; Shou, L.; Li, B. Genomic Characterization of Phage ZP3 and Its Endolysin LysZP with Antimicrobial Potential against *Xanthomonas oryzae* pv. *oryzae*. *Viruses* **2024**, *16* (9), 1450.
(50) Sisson, H. M.; Fagerlund, R. D.; Jackson, S. A.; Briers, Y.; Warring, S. L.; Fineran, P. C. Antibacterial Synergy between a Phage Endolysin and Citric Acid against the Gram-Negative Kiwifruit Pathogen *Pseudomonas syringae* pv. *actinidiae*. *Appl. Environ. Microbiol.* **2024**, *90* (3), e01846−23.
(51) Soontarach, R.; Srimanote, P.; Voravuthikunchai, S. P.; Chusri, S. Antibacterial and Anti-Biofilm Efficacy of Endolysin LysAB1245 against a Panel of Important Pathogens. *Pharmaceuticals* **2024**, *17* (2), 155.
(52) Sitthisak, S.; Voravuthikunchai, S. P.; Chusri, S. Engineering of a novel chimeric endolysin with enhanced antibacterial activity against multidrug-resistant Acinetobacter baumannii. *Sci. Rep.* **2023**, *13*, 7470.
(53) Garcia-Torres, S.; Henrich, D.; Verboket, R. D.; Marzi, I.; Hahne, G.; Kempf, V. A. J.; Göttig, S. Bactericidal Effect of a Novel Phage Endolysin Targeting Multidrug-Resistant Acinetobacter baumannii. *Antibiotics* **2025**, *14*, 162.
(54) Antonova, N. P.; Vasina, D. V.; Grigoriev, I. V.; Laishevtsev, A. I.; Kapustin, A. V.; Savinov, V. A.; Vorobev, A. M.; Aleshkin, A. V.; Zackharova, A. A.; Remizov, T. A.; Makarov, V. V.; Yudin, S. M.; Gushchin, V. A. Pharmacokinetic and Preclinical Safety Studies of an Endolysin-Based Therapeutic for Intravenous Administration. *Int. J. Antimicrob. Agents* **2024**, *64* (5), 107328.
(55) Yao, F.; Wu, X.; Liao, Y.; Yan, Q.; Li, Y. Smart Chimeric Lysin ClyC-Loaded Alginate Hydrogel Reduces *Staphylococcus aureus*-Induced Bone Infection. *Front. Mater.* **2021**, *8*, 763297.

https://doi.org/10.1021/acsomega.6c00294
ACS Omega 2026, 11, 35326−35336